Electrical contacts to monolayer black phosphorus: A first-principles investigation

Kui Gong,[1,2] Lei Zhang,[2,*] Wei Ji,[3] and Hong Guo[2]

[1]*School of Materials Science and Engineering, University of Science and Technology Beijing, Beijing, 100083, People's Republic of China*

[2]*Department of Physics, McGill University, Montreal, H3A 2T8, Canada*

[3]*Department of Physics and Beijing Key Laboratory of Optoelectronic Functional Materials and Micro-nano Devices, Renmin University of China, Beijing 100872, China*

(Received 14 May 2014; revised manuscript received 31 July 2014; published 23 September 2014)

We report first-principles theoretical investigations of possible metal contacts to monolayer black phosphorus (BP). By analyzing lattice geometry, five metal surfaces are found to have minimal lattice mismatch with BP: Cu(111), Zn(0001), In(110), Ta(110), and Nb(110). Further studies indicate Ta and Nb bond strongly with monolayer BP causing substantial bond distortions, but the combined Ta-BP and Nb-BP form good metal surfaces to contact a second layer BP. By analyzing the geometry, bonding, electronic structure, charge transfer, potential, and band bending, it is concluded that Cu(111) is the best candidate to form excellent Ohmic contact to monolayer BP. The other four metal surfaces or combined surfaces also provide viable structures to form metal/BP contacts, but they have Schottky character. Finally, the band bending property in the current-in-plane (CIP) structure where metal/BP is connected to a freestanding monolayer BP, is investigated. By both work function estimates and direct calculations of the two-probe CIP structure, we find that the freestanding BP channel is *n* type.

DOI: 10.1103/PhysRevB.90.125441 PACS number(s): 73.40.Ns, 73.20.At, 73.22.−f, 81.05.Hd

I. INTRODUCTION

Two-dimensional (2D) layered materials such as graphene and transition-metal dichalcogenides (TMDC) have attracted great attention [1–6] as emerging device materials for nanoelectronics due to their novel mechanical, electrical, and optical properties. Most recently, layered black phosphorus (BP), a new and apparently stable elementary 2D material, has been successfully fabricated experimentally [7–11]. BP is an allotrope of phosphorus and can be mechanically exfoliated since the layers of BP are held together by van der Waals (vdW) interaction [12]. Different from graphene, the atoms in a single layer BP are not sitting in a flatland: Instead they form a buckled hexagonal structure by covalence bonds [8], as shown in Fig. 1(a). Few-layer BP has been predicted as an ideal direct band-gap material at the Γ point [13], a property that is very important for electronic and optical applications. From the point of view of switching devices, a major advantage of monolayer BP over graphene is that BP has an intrinsic band gap and graphene does not. The material processes in order to create a band gap in graphene are typically detrimental to the properties. Few-layer BP field-effect transistors (FET) having high mobility at around 1000 $cm^2\ V^{-1}\ s^{-1}$, has been reported experimentally [7,9–11]. However, a large Schottky barrier for *n*-doped multilayer BP FET was found to seriously and detrimentally affect the current-voltage characteristics at small bias [7] in the experimental device. Indeed, in both the traditional microelectronics as well as the emerging nanoelectronics, designing proper metal-semiconductor contacts is a crucial problem of device physics [14–16]. A large potential barrier or Schottky barrier at the metal-semiconductor contact has a significant negative influence on charge transport in FETs.

For emerging nanomaterials such as carbon nanotubes [17,18], graphene [19–21], and TMDC [22–26], tremendous theoretical and experimental efforts have been devoted to understand the metal contacts. On the other hand, the metal-BP contacts have not received systematic investigation so far, and it is the purpose of this work to fill the void. In particular, we aim to determine metal-BP contacts that are Ohmic in order for BP to realize its full potential as a new and emerging electronics material.

Using the density functional theory (DFT) total energy approach, we have systematically investigated atomic structures of monolayer BP on several important metal substrates including Ta(110), Nb(110), Cu(111), Zn(0001), and In(110). These metal surfaces cover a substantial range of work functions and have relatively minimal lattice mismatch with BP, therefore one expects them to serve as possible contact material for BP. We find that monolayer BP are stable on pristine Cu, Zn, and In substrates. For Ta and Nb, the strong interaction between BP and Ta/Nb induces substantial P-P bond distortions in the BP; as such these metals do not make good contacts to monolayer BP. On the other hand, we found that a bilayer BP makes excellent contact to Ta/Nb substrates. For the materials we investigated, it is predicted that the Cu/BP contact has a very good Ohmic character. Finally, the band bending property in the current-in-plane (CIP) structure where metal/BP is connected to a freestanding monolayer BP, is investigated. By both work function estimates and direct calculations of the two-probe CIP structure, we find that the freestanding BP channel of the CIP device is *n* type without further doping.

The rest of the paper is organized as follows. In Secs. II and III, structural relaxations of freestanding BP and metal/BP contacts are presented, respectively. From the atomic structure, in Sec. IV the electronic properties of the metal/BP contacts are determined. To confirm the band bending properties, Sec. V presents a different band bending analysis—this time based on the current-in-plane open structure using DFT carried out within the Green's function formalism. Finally, the paper is summarized in Sec. VI.

*zhanglei@physics.mcgill.ca

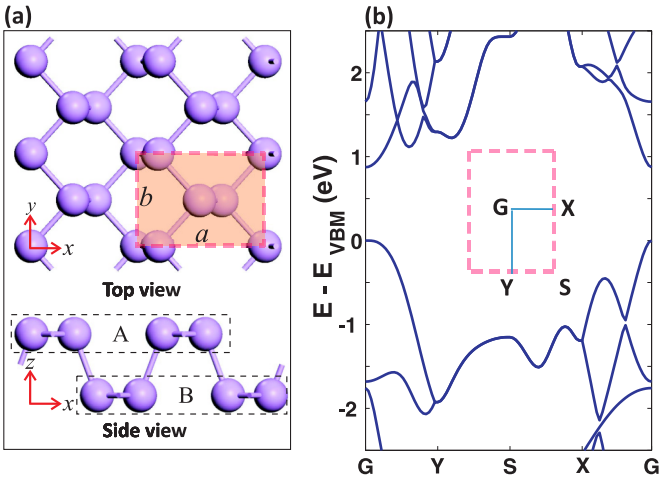

FIG. 1. (Color online) (a) Top and side view of monolayer BP. The shadowed area with four P atoms is a unit cell of monolayer BP. In the side view, atoms in monolayer BP are classified as A/B sublayers. (b) The calculated band structure of monolayer BP and its Brillouin zone with high symmetry points.

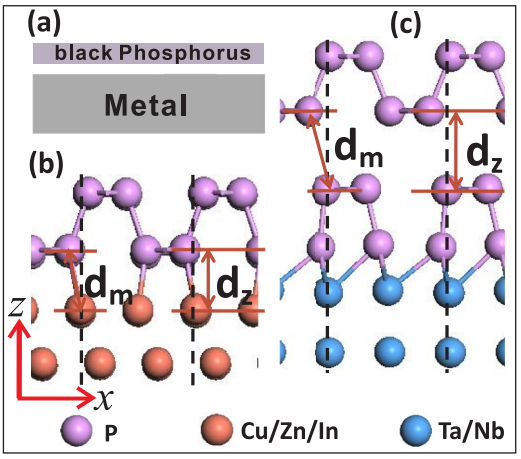

FIG. 2. (Color online) (a) Schematic plot of the monolayer BP and metal contact region. (b) Side view of monolayer BP absorbed on Cu(111), Zn(0001), and In(110) metal surfaces at the contact region. (c) Side view of monolayer BP absorbed on TaP or NbP electrode at the contact region. The dashed line in panels (b) and (c) indicates the supercell in the xz plane.

II. COMPUTATION METHOD AND STRUCTURAL RELAXATION OF BP

Our DFT calculations are carried out with the projector augmented wave [27,28] and the optB88-vdW method [29,30], where van der Waals interaction was considered at the vdW-DF level with optB88 for the exchange functional, as implemented in the Vienna ab initio simulation package (VASP) [31]. The lattice constants of metals are directly taken from experimental values while the lattice constants of freestanding monolayer and bilayer BP are obtained by structure relaxation. To investigate the metal/BP contact, we have chosen a supercell that contains a slab of five layers of metal atoms, a few layers of BP sheets absorbed on the metal slab, and a vacuum region 15 Å thick. The dipole correction has been included to avoid spurious interactions between periodic images of the slab. For structure relaxation, we fixed the atoms in the two bottom metal layers at their respective bulk position, while all other atoms are fully relaxed until the residual force on each atom is smaller than 0.01 eV/Å. A fine k-mesh density at 0.08/Å and energy cutoff at 500 eV were used to ensure numerical accuracy. The relaxed monolayer BP is shown in Fig. 1(a) and we found the lattice constant to be $a = 4.58$ Å and $b = 3.32$ Å, in agreement with Ref. [13]. For simplicity of discussion, in the following we shall call the two sublayers in Fig. 1(a) A and B (see side view). Figure 1(b) plots the Brillouin zone and the calculated band structure showing a direct gap of 0.89 eV.

III. STRUCTURES OF METAL/BP CONTACTS

Having determined the structure of freestanding monolayer BP, we now calculate the structure of the metal/BP contact as schematically shown in Fig. 2(a). As a first design rule of the metal/BP contact, we consider metals having a lattice plane that can match the BP structure because a large mismatch induces strain to distort BP. As monolayer BP is not a perfect honeycomb structure, only a few metals were found to nicely lattice match BP. Next, we note that the puckered structure of BP has smaller elastic modulus along the x direction [13] [see Fig. 1(a)], indicating that structure deformation can easily occur along x which is not good for our purpose. Indeed, we found that monolayer BP adsorbed on Al(111) and Sc(0001) surfaces have three and four BP unit cells per supercell along the x direction, and the relaxed metal/BP structure has significant P-P bond distortions. Therefore, a second design rule is to search metal/BP structures that have one or two BP unit cells per supercell along the x direction. After going through the periodic table, we choose metals Ta(110), Nb(110), Cu(111), Zn(0001), and In(110) as candidates for the metal/BP contacts which cover a wide range of work functions and have relatively minimal lattice mismatch with BP.

For each possible candidate of metal/BP contacts, there are a total of seven different initial configurations to be investigated: three for (111) and two for either (110) or (0001) surfaces. From these initial configurations, the most stable metal/BP structures are found by DFT total energy relaxation, shown in Figs. 2(b) and 2(c). We find that monolayer BP can only perfectly match with In(110), Cu(111), and Zn(0001) surfaces without significant P-P bond distortion, in the form of (1×3), (1×3), and (1×4) unit cells, respectively, as shown in Fig. 2(b). For Ta(110) (1×1) and Nb(110) (1×1) surfaces, it turns out the interaction between P atoms and Ta/Nb atoms is very strong and, as a result, the absorbed monolayer BP is no longer intact due to the presence of broken P-P bonds. Nevertheless, because these two metal surfaces have a very small mismatch with the BP atomic structure, i.e., (1×1) cell, it is still possible to design good metal/BP contacts. Namely, and as shown in Fig. 2(c), when a bilayer BP is in contact with Ta or Nb surfaces, the lower BP layer plus the metal form a *combined substrate* to contact the upper BP layer. The combined substrates are denoted by TaP and NbP in the rest of this paper. We found that a monolayer BP forms very good contact to TaP and NbP.

The calculated equilibrium bonding lengths, binding energies, and work functions for all the metal/BP contacts

TABLE I. Supercell representing the super structure of BP matching with metal substrates. ($n \times m$) denotes that there are n and m BP unit cells along the x and y directions, respectively. The average distance d_z is the equilibrium separation in the z direction between the monolayer BP and the topmost substrate layer after structure relaxation. For simplicity of notation, the interlayer distance for bulk BP is also denoted as d_z in the table. d_m is the shortest bond length between the monolayer BP atoms and the topmost atoms of substrate as shown in Figs. 2(b) and 2(c). E_b is the binding energy per BP unit cell between the monolayer BP and a given substrate. W is work functions of absorbed monolayer BP including the freestanding one (the first column), respectively. ΔE_F is the Fermi level shift of freestanding BP at the band bending region.

	BP	Ta	Cu	Zn	In	TaP	NbP
Supercell		(1×1)	(1×3)	(1×4)	(1×3)	(1×1)	(1×1)
d_z (Å)	3.20	1.76	2.31	2.87	3.00	3.04	3.04
d_m (Å)		2.44	2.36	2.76	3.11	3.55	3.19
E_b (eV)		4.89	1.30	0.64	0.52	0.50	0.50
W (eV)	5.16[a]		4.68	4.51	3.93	4.34	4.41
ΔE_F (eV)			−0.48	−0.65	−1.23	−0.82	−0.75

[a]5.04 for HSE functional.

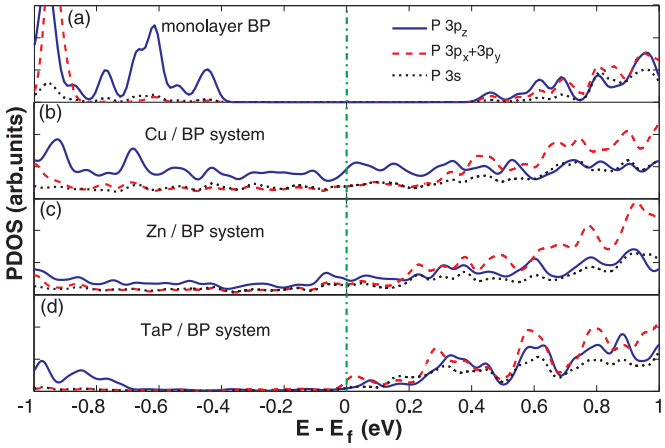

FIG. 3. (Color online) PDOS of P atoms, in (a) the monolayer BP, (b) the Cu/BP system, (c) the Zn/BP system, and (d) the TaP/BP system (the P atoms in the top layer). The blue solid line, red dashed line, and black dotted line represent the $3p_z$ orbital, $3p_x + 3p_y$ orbital, and $3s$ orbital of top layer P atoms as indicated by the legend in (a). The vertical green dashed line indicates the Fermi level.

are summarized in Table I. The average distance between the substrate and the BP layer along the z axis is d_z; the shortest bond between the P atoms and the substrate atoms is d_m (see Fig. 2). We characterize the contact strength using the metal/BP binding energy per BP unit cell defined by $E_b = (E_{\rm BP} + E_{\rm sub} - E_{\rm BP\text{-}sub})/n$, where $E_{\rm BP\text{-}sub}$ is the total energy of BP absorbed on substrate, and $E_{\rm BP}, E_{\rm sub}$ are the total energies of BP and substrate, respectively (obtained from the relaxed structure). Here n gives out the number of BP unit cells in the superstructure. Among the pure metal/BP contacts (Cu,Zn,In), Cu/BP has the smallest $d_z = 2.31$ Å and $d_m = 2.36$ Å, and the largest binding energy $E_b = 1.30$ eV. Three other contacts, In/BP, TaP/BP, and NbP/BP, have almost the same d_z and E_b suggesting that they have similar contact properties. For Ta/BP, $E_b = 4.89$ eV which is much larger than other metal/BP contacts and its $d_z = 1.7$ Å which is much smaller than others: This is because each P atoms is bonded to two or more Ta atoms in Ta/BP. A Similar situation is found for the Nb substrate (not listed in Table I). Such a strong bonding in Ta/BP and Nb/BP induces P-P distortions, making them unsuitable for metal/BP contacts. On the other hand, for the combined contacts TaP/BP and NbP/BP, $d_z = 3.04$ Å which is large enough such that P-P bonds in the upper BP [see Fig. 2(c)] are not broken and, at the same time, this value is smaller than $d_z = 3.20$ Å of the bulk BP, strongly indicate that the combined substrates can make good metal/BP contacts. In the following we quantify properties of the metal/BP contacts using partial density of states (PDOS), charge density, and electronic potential using Cu, Zn, and TaP substrates as other contacts have similar properties.

IV. ELECTRONIC STRUCTURE OF METAL/BP CONTACTS

Having obtained the atomic structures of the metal/BP contacts, we now investigate their electronic properties. Figure 3 plots the calculated PDOS projected on selected orbitals of the P atoms for monolayer BP, Cu/BP, Zn/BP, and TaP/BP. The PDOS of freestanding monolayer BP [Fig. 3(a)] has a gap around the Fermi level: Consistent with its band structure [Fig. 1(b)], the valence state is dominated by the $3p_z$ state while the bottom conduction PDOS is contributed by all types of $3p$ orbitals. The PDOS of Cu/BP, Zn/BP, and TaP/BP has a metallic character as shown in Figs. 3(b)–3(d). From observing the peak of $3p_x + 3P_y$ PDOS, we know the Fermi level of Cu/BP and Zn/BP moves upward by about 0.1 and 0.2 eV with respect to the bottom conduction band of the freestanding BP, respectively. The PDOS of Cu/BP [Fig. 3(b)] near the Fermi level is much lager than that of Zn/BP [Fig. 3(c)] due to a significant increase of contribution from the $3p_z$ states. Since the Cu-BP bonding distance [d_z; see Fig. 2(b) and Table I) is significantly smaller than that of Zn-BP, the $3p_z$ states of P atoms have much stronger interaction with the $3d$ states of Cu than with Zn. As a result, Cu/BP is a better contact than Zn/BP since good device contacts should maximize overlap between states at either side of the contact interface. As for the combined contact TaP/BP [Fig. 3(d)], the in-plane states $3p_x$,$3p_y$ play a more important role than the $3p_z$ state in comparison to Cu and Zn. This is because of Bernal stacking of the top BP layer and the TaP [13], and as a result the overlap of in-plane $3p_{x/y}$ between the two BP layers is much stronger than that of the $3p_z$ states.

The interaction between BP and metal is quantified by calculating the charge density. To compare different contacts, we integrate the density along the y direction [see Fig. 1(a)] and normalize it per unit cell of BP. The corresponding results for Cu/BP and Zn/BP are presented in the left panels of Figs. 4(a) and 4(e), respectively. Here we clearly observe that the normalized charge density ρ at the interface of Cu/BP is much larger than that of the Zn/BP interface (by the color coding). As usual, interface dipoles are formed due to interaction of charge carriers at the interface which is visualized from the electron rearrangement defined as

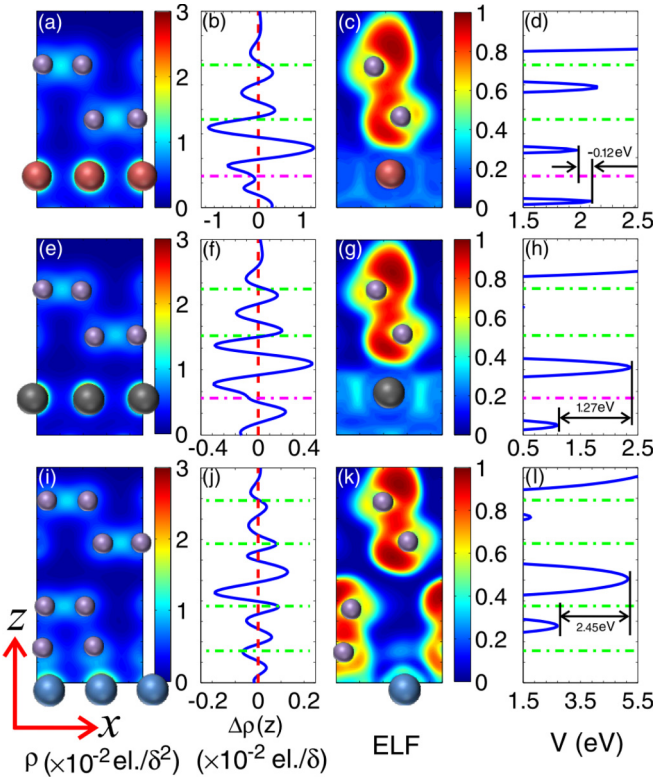

FIG. 4. (Color online) Electronic structure at the interface of the contact region: (a)–(d) for Cu substrate, (e)–(h) for Zn substrate, and (i)–(l) for TaP substrate. The left side contour plots represent charge density ρ which is integrated in the y direction and normalized to one BP unit cell. The unit is number of electrons per area (denoted as el./δ^2) The middle panels (b), (f), and (j) are charge density difference $\Delta\rho(z)$, which is integrated over the x and $y$directions and normalized to one BP unit cell. The middle panels (c), (g), and (k) are contour plots of the electron localization function (ELF) in a slice along the y axis that crosses both P atoms and metal atoms. The panels (d), (h), and (l) are average local potential V. The average potential barriers at the BP and metal interface are also indicated. δ is the length of the real-space grid, equal to 0.065 Å. The green dashed lines represent the position of each average P atom layer and the pink dashed lines represent the position of the average metal surface after structure relaxation.

$\Delta\rho(z) = [\rho_{\text{sub-BP}}(z) - \rho_{\text{sub}}(z) - \rho_{\text{BP}}(z)]/n$, where $\rho_{\text{sub}}(z)$ and $\rho_{\text{BP}}(z)$ are densities of substrate and monolayer BP. Here, negative (positive) $\Delta\rho(z)$ stands for charge depletion (accumulation) in the x-y plane, and plotted in Figs. 4(b) and 4(f). The large net charge accumulation between the B sublayer of BP [lower P atoms in BP; see Fig. 1(a)] and the topmost layer of metal suggests that covalence bonds have been formed. In addition, the magnitude of $\Delta\rho(z)$ in Cu/BP is twice as large as that of Zn/BP, indicating that the strength of the covalence bond of Cu/BP is significantly larger than that in Zn/BP.

A vivid physical picture of the chemical bonds at the metal/BP interface can be established by investigating the electron localization function (ELF) for the slice that crosses both P atoms and metal atoms in the y direction, shown in Figs. 4(c), 4(g), adn 4(k). Physically, ELF measures the extent of spatial localization of a reference electron, with upper limit ELF($\mathbf{r}$) = 1 corresponding to perfect localization (lone pairs) and ELF($\mathbf{r}$) = 1/2 corresponding to electron-gas-like pairs [32]. Clearly, from Fig. 4(c) the upper P atom [A layer in Fig. 1(a)] has a significantly larger ELF than the lower P atom [B layer in Fig. 1(a)]; this is reasonable because the lower P atom is closer to Cu contact, which makes their electrons more delocalized. A similar conclusion is true for the Zn/BP contact, but the ELF of Zn/BP is larger than that of Cu/BP—again indicating a weaker covalent bond between Zn-BP than Cu-BP. As for the combined contact TaP/BP whose ELF is shown in Fig. 4(k), there is a delocalized region (dark blue) between the top BP layer and TaP, indicating that the chemical bond between the two BP layers is very weak and the dominating interaction at the TaP/BP interface is largely via the vdW force. This is why the dipoles between the two BP layers in Fig. 4(j) is three to six times smaller than that between BP and Zn or Cu.

From the calculated electronic structure, we obtain a most important parameter for charge injection from metal to BP, namely, the potential barrier at the metal/BP interface. The electronic potential (ionic and Hartree contributions) averaged over the x-y plane across the lower P atoms of the BP which are in direct contact to the metal [e.g., the B sublayer; see Fig. 1(a)], is shown in Figs. 4(d) and 4(h) for Cu/BP and Zn/BP. For TaP/BP, the potential is averaged over the P atoms in direct contact to the TaP substrate as shown in Fig. 4(l). Since ionic contribution is included, the highest averaged potential appears at the middle of each two neighboring atomic layers. We define a quantity ΔV to be the difference between highest averaged potential at the contact interface and the highest averaged potential at the metal surface, as indicated by the black arrows. It comes as a pleasant surprise that $\Delta V = -0.12$ eV is *negative* for Cu/BP [Fig. 4(d)], indicating electrons can be easily injected from Cu to the BP without any potential barrier. On the other hand, Zn/BP and TaP/BP all have positive ΔV at 1.27 and 2.45 eV, respectively. We conclude that Cu/BP is an excellent Ohmic contact and the other contacts have large potential barriers but electron injection into BP is still possible due to nonzero PDOS at the Fermi level.

V. BAND BENDING IN CURRENT-IN-PLANE STRUCTURES

In the previous sections, we determined the electronic structures of several metal/BP contacts and concluded that Cu/BP is the best in the sense that Cu forms Ohmic contact to BP. Moving forward and anticipating Cu/BP to be used as the contact (electrode) to form two-probe BP transport junctions, an important issue is the band bending between Cu/BP (and other metal/BP) and a freestanding BP. In this section we qualitatively and quantitatively determine the band bending using the CIP device model schematically plotted in Fig. 5(a). Here, the metal/BP extends to $z = -\infty$ and the free BP to $z = +\infty$, with an interface in the middle where band bending occurs due to charge transfer.

First, the band bending can be estimated by the Fermi level difference [20] between the metal/BP and the freestanding BP: $\Delta E_F = W - W_{\text{BP}}$ where W and W_{BP} are the work functions of metal/BP and freestanding BP, respectively. Note that the work function of BP is defined from just above the valence band. If $\Delta E_F > 0$, electrons transfer from the freestanding BP to the

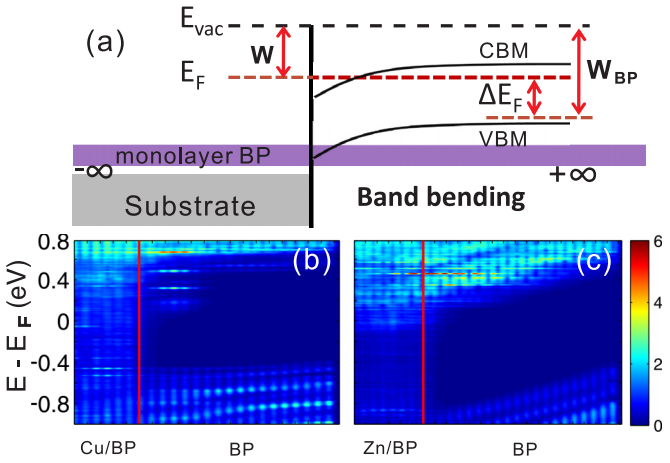

FIG. 5. (Color online) (a) Schematic plot of a CIP device where the metal/BP contact is connected to a freestanding BP channel extending to the right. W and W_{BP} denote work functions of the metal/BP and the freestanding BP, respectively. The black lines qualitatively indicate the band bending. (b) and (c) plot the calculated local density of states (LDOS) in color coding for CIP devices with Cu/BP and Zn/BP electrodes, respectively. The red line indicates the boundary of metal/BP and the freestanding monolayer BP. In the LDOS plot, only the contributions from BP atoms are plotted in the metal/BP region for clarity purposes.

metal/BP and the channel is p type. When $\Delta E_F < 0$, the BP channel is n type. As tabulated in Table I, we found $\Delta E_F < 0$ for all five viable metal/BP contacts, hence these contacts tend to produce n-type CIP devices without further doping. The Cu/BP contact has the smallest band bending, $\Delta E_F = -0.48$ eV. Interestingly, TaP/BP and NbP/BP contacts also have rather small bending, $\Delta E_F \approx -0.7$ to -0.8 eV. From the CIP point of view, the smaller the shift the better the contact.

The above values were obtained by optB88-vdW [29,30] which tends to under estimate the band gap of semiconductors. We have also used the Heyd-Scuseria-Ernzerhof (HSE) hybrid functional [33] to calculate freestanding monolayer BP and obtained a work function $W_{\mathrm{BP}} = 5.04$ eV. This is to be compared with the optB88-vdW result of 5.16 eV (see Table I). For the metal/BP, HSE calculation becomes very expensive. Hence, using the optB88-vdW value for Cu/BP, $W = 4.68$ eV (Table I) and HSE value for BP, we estimate $\Delta E_F = W - W_{\mathrm{BP}} = -0.36$ eV which is still negative and small. We conclude that the band bending picture is qualitatively consistent between the optB88-vdW estimate and the partially HSE estimate.

The above estimate was done by calculating the metal/BP and freestanding BP *separately*. A better approach is to determine the band bending directly for the CIP geometry as a whole, i.e., by a two-probe transport analysis. To this end we carry out DFT analysis within the Keldysh nonequilibrium Green's function (NEGF) formalism [34], as implemented in the quantum transport package NANODCAL [34–36]. Since the CIP device is actually an infinitely large system, we divide it into three regions: the left electrode which is the semi-infinite metal/BP, the right electrode which is the freestanding monolayer BP, and the central region consisting of the interface region between the metal/BP and free BP where band bending occurs. For technical details of the NEGF-DFT theory, we refer interested readers to Ref. [34]. In our NEGF-DFT self-consistent calculations, a linear combination of atomic orbital basis at the double-ζ polarization level is used to expand physical quantities; the standard norm-conserving nonlocal pseudopotentials [37] are used to define the atomic core; the local density approximation is used for the exchange-correlation potential [38].

We apply the NEGF-DFT formalism to self-consistently calculate the electronic structure of the CIP two-probe model with Cu/BP and Zn/BP as examples. Note that the CIP geometry has no translational symmetry along the transport direction [from left to right, Fig. 5(a)], the concept of band structure is not well defined. Therefore we investigate band bending by visualizing the local density of states (LDOS) versus the coordinate along transport direction (z), shown in Figs. 5(b) and 5(c) by color coding. The band gap in the free BP region (to the right of the red vertical line) is clearly visible. Interestingly, the LDOS corresponding to the valence bend up for both Cu/BP and Zn/BP indicating that the free BP is n type, in agreement with the above band bending estimates using the work functions. In comparison with the Cu/BP CIP device, the curvature of band bending in Zn/BP is much larger. Correspondingly, electron injection from Zn/BP to the free BP will encounter a lager potential barrier. Finally, we note that there exist some interfacial states inside the BP gap but above the Fermi energy.

VI. SUMMARY

In summary, by atomistic calculations we have systematically investigated the possible metal/BP contacts which allows us to design viable structures for future device applications. Our design rule starts from selecting metals that have a lattice plane matching the BP structure so that strain at the metal/BP interface is minimized. Of the five metals that satisfy this condition, Ta and Nb are found to form strong bonds with monolayer BP to generate substantial P-P bond distortions in the BP; for this reason we further considered TaP and NbP as combined metal substrates. We predict that monolayer BP absorbed on Cu(111), Zn(0001), In(110), TaP(110), and NbP(110) form viable metal/BP contacts. From the calculated geometry, bonding structure, density of states, charge transfer, and potential barriers at the metal/BP interface, we predict that Cu/BP is an excellent Ohmic contact and the rest are Schottky contacts where the electronic potential barrier increases with the averaged distance between monolayer BP and the metal substrate. For the CIP device model where a freestanding monolayer BP is the channel material, the estimated band bending property suggests an intrinsically n-type device for all the contacts and, in particular, the Cu/BP is the most ideal contact to the freestanding BP channel. Therefore we conclude that Cu(111) is the best choice as an electrode metal for monolayer BP electronic device applications. The theoretical predictions of this work should be experimentally testable. Note that in this work, we focused on metal/BP contacts where the metal is nonmagnetic. Magnetic metal such as fcc Ni has lattice constants close to that of Cu, and thus would be very interesting to investigate for spin injection into BP.

ACKNOWLEDGMENTS

This work is supported by NSERC of Canada and University Grant Council (Contract No. AoE/P-04/08) of the Government of HKSAR (H.G.), the China Scholarship Council (K.G.), and the National Natural Science Foundation (NSFC), Grant No. 11274380 (W.J.). We thank CLUMEQ, Calcul Québec, and Compute Canada for providing computation facilities.

[1] K. S. Novoselov, A. K. Geim, S. V. Morozov, D. Jiang, Y. Zhang, S. V. Dubonos, I. V. Grigorieva, and A. A. Firsov, Science **306**, 666 (2004).
[2] A. Splendiani, L. Sun, Y. Zhang, T. Li, J. Kim, C. Chim, G. Galli, and F. Wang, Nano Lett. **10**, 1271 (2010).
[3] K. F. Mak, C. Lee, J. Hone, J. Shan, and T. F. Heinz, Phys. Rev. Lett. **105**, 136805 (2010).
[4] M. Xu, T. Liang, M. Shi, and H. Chen, Chem. Rev. **113**, 3766 (2013).
[5] S. Lebègue, T. Björkman, M. Klintenberg, R. M. Nieminen, and O. Eriksson, Phys. Rev. X. **3**, 031002 (2013).
[6] S. Lebègue and O. Eriksson, Phys. Rev. B **79**, 115409 (2009).
[7] L. Li, Y. Yu, G. J. Ye, Q. Ge, X. Ou, H. Wu, D. Feng, X. H. Chen, and Y. Zhang, Nat. Nanotech. **9**, 372 (2014).
[8] A. Brown and S. Rundqvist, Acta. Crystallogr. **19**, 684 (1965).
[9] S. P. Koenig, R. A. Doganov, H. Schmidt, A. H. C. Neto, and B. Özyilmaz, Appl. Phys. Lett. **104**, 103106 (2014).
[10] M. Buscema, D. J. Groenendijk, S. I. Blanter, G. A. Steele, H. S. J. van der Zant, and A. Castellanos-Gomez, Nano Lett. **14**, 3347 (2014).
[11] H. Liu, A. T. Neal, Z. Zhu, D. Tománek, and P. D. Ye, ACS Nano. **8**, 4033 (2014).
[12] E. O. Noläng, O. Eriksson, and B. Johansson, J. Phys. Chem. Solids **51**, 1025 (1990).
[13] J. Qiao, X. Kong, Z.-X. Hu, F. Yang, and W. Ji, Nat. Commun. **5**, 4475 (2014).
[14] F. Léonard and A. A. Talin, Phys. Rev. Lett. **97**, 026804 (2006).
[15] Y. F. Lin and W. B. Jian, Nano Lett. **8**, 3146 (2008).
[16] B. L. Sharma, *Metal-Semiconductor Schottky Barrier Junctions and Their Applications* (Springer, New York, 1984).
[17] Z. Chen, J. Appenzeller, J. Knoch, Y.-m. Lin, and P. Avouris, Nano Lett. **5**, 1497 (2005).
[18] N. Nemec, D. Tománek, and G. Cuniberti, Phys. Rev. Lett. **96**, 076802 (2006).
[19] G. Giovannetti, P. A. Khomyakov, G. Brocks, V. M. Karpan, J. van den Brink, and P. J. Kelly, Phys. Rev. Lett. **101**, 026803 (2008).
[20] P. A. Khomyakov, G. Giovannetti, P. C. Rusu, G. Brocks, J. van den Brink, and P. J. Kelly, Phys. Rev. B **79**, 195425 (2009).
[21] M. Bokdam, P. A. Khomyakov, G. Brocks, Z. Zhong, and P. J. Kelly, Nano Lett. **11**, 4631 (2011).
[22] I. Popov, G. Seifert, and D. Tománek, Phys. Rev. Lett. **108**, 156802 (2012).
[23] W. Liu, J. Kang, D. Sarkar, Y. Khatami, D. Jena, and K. Kaustav Banerjee, Nano Lett. **13**, 1983 (2013).
[24] W. Chen, E. J. G. Santos, W. Zhu, E. Kaxiras, and Z. Zhang, Nano Lett. **13**, 509 (2013).
[25] C. Gong, L. Colombo, R. M. Wallace, and K. Cho, Nano Lett. **14**, 1714 (2014).
[26] S. Das, H.-Y. Chen, A. V. Penumatcha, and J. Appenzeller, Nano Lett. **13**, 100 (2013).
[27] P. E. Blöchl, Phys. Rev. B. **50**, 17953 (1994).
[28] G. Kresse and D. Joubert, Phys. Rev. B **59**, 1758 (1999).
[29] M. Dion, H. Rydberg, E. Schröder, D. C. Langreth, and B. I. Lundqvist, Phys. Rev. Lett. **92**, 246401 (2004).
[30] J. Klimeš, D. R. Bowler, and A. Michaelides, Phys. Rev. B **83**, 195131 (2011).
[31] G. Kresse and J. Furthmüller, Phys. Rev. B **54**, 11169 (1996).
[32] A. D. Becke and K. E. Edgecombe, J. Chem. Phys. **92**, 5397 (1990).
[33] J. Paier, M. Marsman, K. Hummer, G. Kresse, I. C. Gerber, and J. G. Ángyán, J. Chem. Phys. **124**, 154709 (2006).
[34] J. Taylor, H. Guo, and J. Wang, Phys. Rev. B **63**, 245407 (2001).
[35] D. Waldron, P. Haney, B. Larade, A. MacDonald, and H. Guo, Phys. Rev. Lett. **96**, 166804 (2006).
[36] For details of the NANODCAL quantum transport package, see http://www.nanoacademic.ca.
[37] L. Kleinman and D. M. Bylander, Phys. Rev. Lett. **48**, 1425 (1982).
[38] J. P. Perdew and Y. Wang, Phys. Rev. B **45**, 13244 (1992).